IEEE Access
Multidisciplinary | Rapid Review | Open Access Journal

Received April 8, 2019, accepted April 21, 2019, date of publication April 29, 2019, date of current version May 14, 2019.

Digital Object Identifier 10.1109/ACCESS.2019.2913552

Mutual Coupling Reduction of a Circularly Polarized Four-Element Antenna Array Using Metamaterial Absorber for Unmanned Vehicles

JUN ZHANG[1], (Member, IEEE), JIANXING LI[2], (Member, IEEE), AND JUAN CHEN[3], (Member, IEEE)

[1]The State Key Laboratory of Bioelectronics, Jiangsu Key Laboratory of Remote Measurement and Control, School of Instrument Science and Engineering, Southeast University, Nanjing 210096, China
[2]School of Electronic and Information Engineering, Xi'an Jiaotong University, Xi'an 710049, China
[3]Shenzhen Research School, Xi'an Jiaotong University, Shenzhen 518057, China

Corresponding author: Jun Zhang (j.zhang@seu.edu.cn)

This work was supported in part by the National Natural Science Foundation of China under Grant 61873066 and Grant 61801369, in part by the Natural Science Foundation of Shaanxi Province under Grant 2018JQ6081, in part by the China Postdoctoral Science Foundation under Grant 2018M631161, in part by the Shaanxi Province Postdoctoral Science Foundation under Grant 2017BSHYDZZ14, in part by the Fundamental Research Funds for the Central Universities under Grant XJTU1191329860, and in part by the Technology Program of Shenzhen under Grant JCYJ20170816100722642.

ABSTRACT A double-layer metamaterial absorber is proposed to suppress the mutual coupling within a circularly polarized (CP) four-element antenna array operating at the Chinese Beidou navigation satellite system (BDS) B3 band, wherein four miniaturized patch antenna elements are positioned in a rotationally symmetric distribution. The single-feed antenna element utilizes simultaneously a thick air substrate to widen the achievable CP bandwidth, four parasitic grounded strips to reduce the size occupation, and a capacitive probe feed to enhance the impedance matching. A wall of the double-layer metamaterial absorber using slotted cross patch structure is introduced in between the four CP antenna elements. An antenna array prototype with an overall footprint size of $0.81\lambda_0 \times 0.81\lambda_0$ (λ_0 denotes the free-space wavelength at 1268 MHz) is implemented and validated experimentally. The measured results in a good agreement with the simulated ones demonstrate a mutual coupling reduction of 11 and 8 dB, for the parallel-directed and orthogonal-directed antenna element pairs across the entire operation band, and meanwhile a good CP performance is also achieved. Details of the design considerations as well as the simulation and measurement results are presented and discussed. The proposed antenna array can be well suited for BDS anti-jam antenna applications in unmanned vehicles.

INDEX TERMS Antenna array, BeiDou navigation satellite system (BDS), circularly polarized (CP) antenna, miniaturized antenna, metamaterial absorber, mutual coupling.

I. INTRODUCTION

It is well known that receivers of global navigation satellite systems (GNSS) are much vulnerable to ambient interferences and intentional jammers as a result of the relatively weak signal strength received on the earth [1]. Therefore, adaptive anti-jam antenna arrays are generally deployed to overcome this drawback by placing radiation pattern nulls in real time towards the arrival angles of undesired interfering signals [2], [3]. To accommodate aperture-sensitive scenarios involving small unmanned vehicles, the anti-jam GNSS arrays having an inter-element separation of less than half wavelength are usually demanded. Hence, a challenging aspect in realizing such an anti-jam array is designing an antenna array that exhibits sufficient inter-element isolation, otherwise the anti-jam capabilities in terms of nulling accuracy and depth would be significantly deteriorated [4], [5].

Recently, many techniques have been reported to decouple various types of linearly polarized (LP) antenna arrays. Employing offsetting branches has been demonstrated to

The associate editor coordinating the review of this manuscript and approving it for publication was Guan-Long Huang.

be an effective method to suppress mutual coupling within planar patch and monopole antenna arrays [6], [7]. Integrating particularly designed impedance matching networks has successfully enhanced isolation between monopole and inverted-F antennas [8], [9]. The effectiveness of defected ground structures and mushroom-like structures exhibiting electromagnetic band-gap (EBG) characteristic has been comprehensively validated in reducing mutual coupling within different antenna arrays, including planar inverted-F antennas [10], slot antennas [11], [12], patch antennas [13], [14], and monopole antennas [15]. Additionally, another increasingly preferred decoupling technique is utilizing metamaterials fulfilled with the use of spiral resonators [16] and split ring resonators [17]–[19] that show a negative equivalent permeability within the operation bands. Yet, few studies can be found in literature to decouple circularly polarized (CP) antennas. The complexity of the coupling mechanism in GNSS arrays comes from the different coupling field distributions caused by the two orthogonal modes responsible for CP generation. In [20], eight arrays of stacked broadside coupled split ring resonators were strategically located and oriented, to simultaneously inhibit the fields contributing to the E-plane and H-plane coupling, and resultantly a mutual coupling reduction of 10 dB was obtained. The realization of this technique is, however, relatively challenging since it requires totally forty vertically placed split ring resonators, and each five of them have to be strictly aligned. A coplanar modified electric-field-coupled (MELC) resonator featuring a negative permittivity has been proposed to enhance the inter-element isolation of a CP antenna array in [21]. Yet, the effective bandwidth is rather narrow.

This paper presents a double-layer metamaterial absorber to improve the inter-element isolation of a four-element BDS antenna array. The array utilizes single-feed miniaturized CP antenna elements and rotationally symmetric distribution, distinguishing it from exiting GNSS arrays [20], [22], [23] that are dual-feed and identically positioned. A wall realized by the double-layer metamaterial absorber, making use of the slotted cross patch structure, is placed symmetrically in between the CP antenna elements. The double-layer metamaterial absorber wall absorbs the space waves between the antenna elements contributing to the mutual coupling, and hence the inter-element isolation is enhanced significantly. The experimental results demonstrate a reduced mutual coupling of 11 dB and 8 dB for the parallel-directed (diagonal) and orthogonal-directed (neighbor) antenna element pairs, respectively. In comparison to that in [20], the proposed mutual coupling suppression technique achieves a comparable isolation enhancement and more simplified realization process.

The rest of this work is arranged as follows. Section II describes the geometric configuration and simulated performance of the stand-alone single-feed miniaturized BDS B3 antenna element. In Section III, the methodology of the proposed double-layer metamaterial absorber wall is introduced, and its effectiveness in reducing the mutual coupling of the four-element CP antenna system is investigated by comparing with those without and with a metallic wall. Section IV shows and discusses the simulated and measured results of an antenna array prototype. A conclusion is finally drawn in Section V. The Ansoft HFSS simulator is used to simulate and optimize the antenna array.

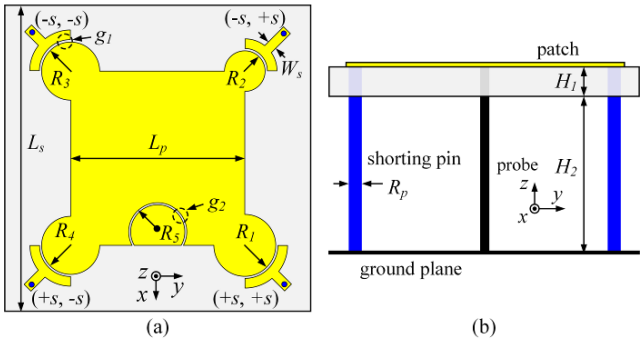

FIGURE 1. Geometry of the proposed single-feed miniaturized CP antenna element. (a) Top view. (b) Side view.

TABLE 1. Optimal parameters of the stand-alone antenna element.

Parameter	H_1	H_2	L_s	L_p	R_1	R_2	R_3
Value (mm)	3.18	14.1	30.0	18.0	3.2	2.1	3.0
Parameter	R_4	R_5	R_p	W_s	s	g_1	g_2
Value (mm)	3.0	2.8	0.5	1.0	13.0	0.2	0.2

II. SINGLE-FEED MINIATURIZED CP ANTENNA ELEMENT

Fig. 1 shows the geometry of the proposed single-feed miniaturized CP antenna element to operate at the BDS B3 band, i.e. 1268.52 ± 10.23 MHz. The antenna is composed of a square patch radiator printed on a readily available Taconic RF-60 substrate ($\varepsilon_r = 6.15$, $\tan\delta = 0.0028$). In detail, four unbalanced circular patches as perturbation segments are loaded onto corners of the patch radiator, to excite a CP wave [24]. To miniaturize the antenna size, rather than using costly high dielectric substrates [22], [23], four parasitic grounded strips are symmetrically loaded along the diagonal lines of the patch radiator. The arc-shaped strip subtended by 90° is coupled to the circular patch, and the tail of the strip is grounded through a shorting pin. Therefore, an LC loading is realized, resulting in a reduced antenna size. However, considering the fact the bandwidth of a patch antenna narrows with decreasing the antenna size, a thick air layer is sandwiched in between the substrate and ground plane, so as to broaden the achievable CP bandwidth [25]. Moreover, an annular gap capacitor is embedded on the patch radiator to compensate the large probe inductance resulted from the thick air substrate, and hence enhances the impedance matching while impacts the already well-behaved CP property negligibly [26]. The optimized parameters of the antenna, obtained after several design iterations, are summarized in Table 1. It should be reminded that a realistic finite

size 190 mm ×190 mm ground plane has been employed in the simulations throughout the paper. The antenna occupies an overall size of 30 mm × 30 mm ×17.3 mm, implying an electrically small footprint, i.e. $\lambda_0/8 \times \lambda_0/8$, where λ_0 is the free-space wavelength at the center frequency of the BDS B3 band, i.e. 1268 MHz. Therefore, besides achieving almost identical reduced footprint, the proposed antenna element outperforms those of the previously reported GNSS arrays, which utilizes relatively complicated dual-feed networks, costly dielectric substrates, or lossy lumped components [20], [22], [23].

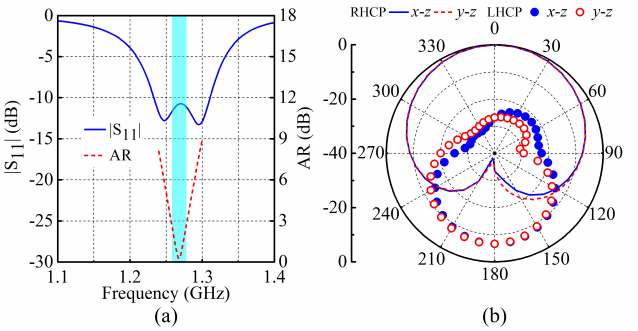

FIGURE 2. Simulated performance of the single-feed miniaturized antenna element. (a) $|S_{11}|$ and boresight AR. (b) Radiation patterns.

The simulated $|S_{11}|$ and boresight axial ratio (AR) of the stand-alone antenna element are illustrated together in Fig. 2(a). It exhibits that an impedance bandwidth ($|S_{11}| < -10$ dB) ranging from 1234 MHz to 1310 MHz and a circular polarization bandwidth (AR < 3 dB) ranging from 1256 MHz to 1280 MHz are obtained, demonstrating that the proposed antenna element is fairly qualified to enclose the entire BDS B3 band. Fig. 2(b) presents the simulated right-hand CP (RHCP) and left-hand CP (LHCP) farfield radiation patterns in both the *x*-*z* and *y*-*z* planes at 1268 MHz, respectively. High CP purity can be apparently observed almost all over the upper hemisphere.

III. MUTUAL COUPLING REDUCTION USING METAMATERIAL ABSORBER WALL

A. MUTUAL COUPLING OF TWO FOUR-ELEMENT CP ANTENNA ARRAYS

This section first presents and compares the inter-element isolation within two differently configured four-element CP antenna arrays, as depicted in Fig. 3. The antenna elements of the Array-I are positioned identically, whereas those of the Array-II are placed in a rotationally symmetric distribution. Both antenna arrays have the same center to center separation denoted as d. To produce radiation nulls towards the arrival angles of interfering signals, the anti-jam GNSS array generally subjects the weight of the reference antenna element to be unit and calculates the weights of other antenna elements adaptively [2], [3], [20]. Hence, both Array-I and Array-II are applicable to the anti-jam GNSS array.

Fig. 4 presents the simulated inter-element isolation of the Array-I and Array-II, respectively, when $d = 95$ mm,

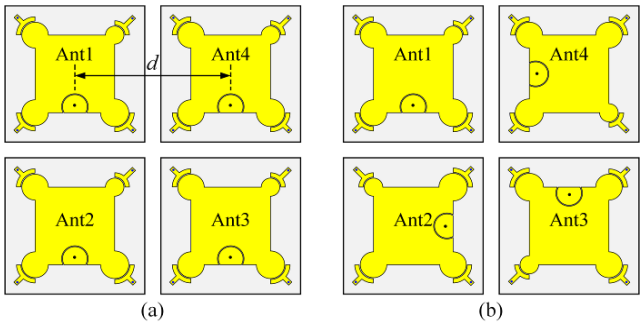

FIGURE 3. Layout of the two differently configured four-element CP antenna arrays. (a) Array-I. (b) Array-II.

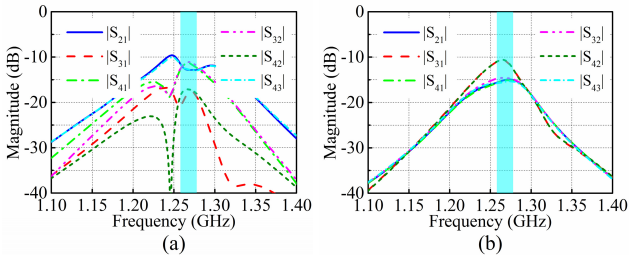

FIGURE 4. Mutual coupling of the two four-element antenna arrays. (a) Array-I. (b) Array-II.

i.e. $0.4\lambda_0$. Each antenna element pair in the Array-I is parallelly positioned. From Fig. 4(a), it can be observed that, across the BDS B3 band, the isolation between neighbor parallel-directed antenna element pairs ($|S_{21}|$, $|S_{41}|$, $|S_{32}|$, and $|S_{43}|$) are below 13 dB, and those of diagonal parallel-directed antenna element pairs ($|S_{31}|$ and $|S_{42}|$) are more than 17 dB, as a result of the relatively larger inter-element separation. Differently, in the Array-II, the neighbor antenna element pairs are orthogonally directed, and the diagonal ones are parallelly positioned. Compared with the Array-I, the neighbor orthogonal-directed antenna element pairs in the Array-II exhibit a higher isolation of above 15 dB, as displayed in Fig. 4(b). This is because the *E*-fields of the neighbor antenna element pairs are always orthogonal to each other. On the other side, due to the closer spacing between the excitation points, the diagonal parallel-directed antenna element pairs in the Array-II show a poorer isolation of more than 10 dB, in comparison to those of the Array-I. To conclude, the overall inter-element isolation of the Array-II generally prevails that of the Array-I. Therefore, as well as to save the simulation time consumption and simplify the antenna array design, the rotationally symmetric configuration is adopted in this work, and only $|S_{11}|$, $|S_{21}|$, and $|S_{31}|$ are discussed in the following analysis.

B. FOUR-ELEMENT ANTENNA ARRAY USING DOUBLE-LAYER METAMATERIAL ABSORBER WALL

Fig. 5 shows the overview of the proposed four-element CP antenna array integrated with a double-layer metamaterial absorber wall. The four CP antenna elements are orthogonally configured at an identical center to center separation

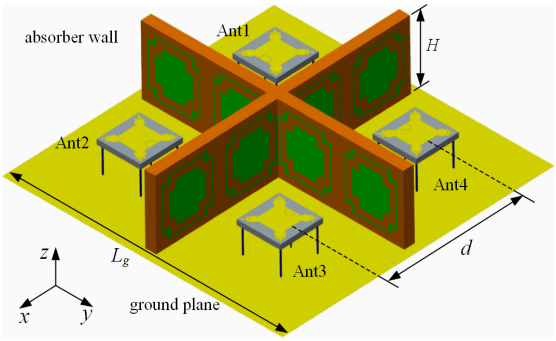

FIGURE 5. Geometry of the proposed four-element CP antenna array integrated with a double-layer metamaterial absorber wall.

$d = 95$ mm, and two pieces of double-layer metamaterial absorber walls with a height of H are symmetrically crossed in between the antenna elements on a $L_g \times L_g = 190$ mm $\times 190$ mm ground plane.

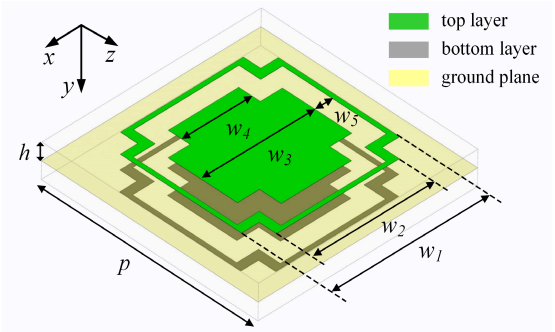

FIGURE 6. Geometry of the proposed double-layer metamaterial absorber cell.

The double-layer metamaterial absorber cell is illustrated in Fig. 6. It is implemented on two-layer FR-4 substrates ($\varepsilon_r = 4.9$, $\tan\delta = 0.025$) with the same thickness $h = 3.7$ mm. Sandwiched in between them is a shared ground plane. Two identical slotted cross patches are printed symmetrically onto the bottom side of the lower substrate and the top side of the upper substrate, respectively. The metamaterial absorber cells, at a period of p, are extended two-dimensionally along both the x- and z-axes. The number of metamaterial absorber cells along the x-axis, i.e. N_x, depends on the total size of the antenna array, while that along the z-axis, i.e. N_z, should be traded off between the requirements on the inter-element isolation and antenna array profile.

Aided by the simulator Ansoft HFSS, the absorption characteristic of the double-layer metamaterial absorber is analyzed and optimized in order to operate at the BDS B3 band. The final determined physical parameters are as follows (unit: mm): $h = 3.7$, $w_1 = 36$, $w_2 = 28$, $w_3 = 26$, $w_4 = 16$, $w_5 = 4$, and $p = 45$. Fig. 7(a) depicts the computational model of the metamaterial absorber cell, wherein the Floquet port and Master/Slave periodic boundary conditions are used. The simulated reflection coefficient $|S_{11}|$ and calculated absorptivity, i.e. $\rho = 1\text{-}|S_{11}|^2$, under a normal incident electromagnetic wave, are presented in Fig. 7(b). It can be

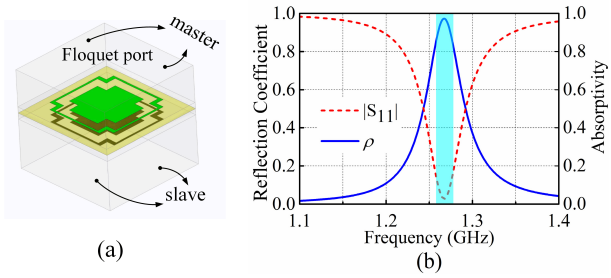

FIGURE 7. (a) Computational model and (b) simulated reflection coefficient $|S_{11}|$ and calculated absorptivity ρ of the metamaterial absorber.

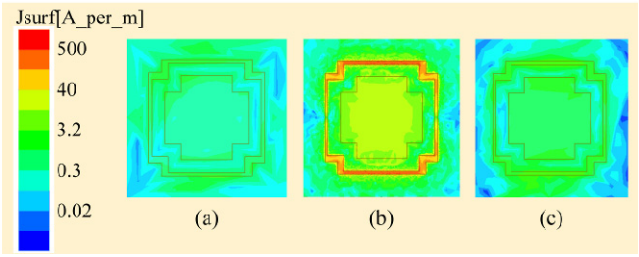

FIGURE 8. Simulated surface current distribution of the metamaterial absorber. (a) 1200 MHz. (b) 1268 MHz. (c) 1300 MHz.

observed that, across the BDS B3 band, the absorptivity stays more than 0.8. Furthermore, Fig. 8 shows the simulated surface current distribution of the metamaterial absorber. Apparently, weak currents are induced both at 1200 MHz and 1300 MHz. Nevertheless, a strong one-wavelength resonance is excited and much currents can be seen surrounding the slotted cross patches at 1268 MHz, implying that most incident electromagnetic waves are efficiently absorbed.

Taking into account the operation frequency band as well as the footprint and height of the antenna array, a double-layer metamaterial absorber wall arrayed by one row and four column cells, i.e. $N_z = 1, N_x = N_y = 4$ is ultimately selected, as shown in Fig. 5. Therefore, the total height of the antenna array is $H = N_z \times p = 45$ mm.

C. MUTUAL COUPLING COMPARISON OF THE FOUR-ELEMENT ANTENNA ARRAY WITH AND WITHOUT METAMATERIAL ABSORBER WALL

For comparison, the four-element antenna array with the proposed double-layer metamaterial absorber wall and with/without a metallic wall made of copper are simulated. The metallic wall is with the same height and length as the metamaterial absorber wall. In Fig. 9(a), it can be seen that the impedance matching of the antenna element is affected significantly by the wall types. Specifically, the $|S_{11}|$, in the presence of the metallic wall, is larger than -10 dB across almost the entire BDS B3 band. The simulated inter-element isolation of the antenna array under the three scenarios are displayed in Figs. 9(b) and 9(c). Without any decoupling wall, the isolation of the neighbor orthogonal-directed antenna element pair, i.e. $|S_{21}|$, is just below -15 dB, whereas that of the diagonal parallel-directed antenna element pair, i.e. $|S_{31}|$, is less than -10 dB. When loaded by the metallic wall,

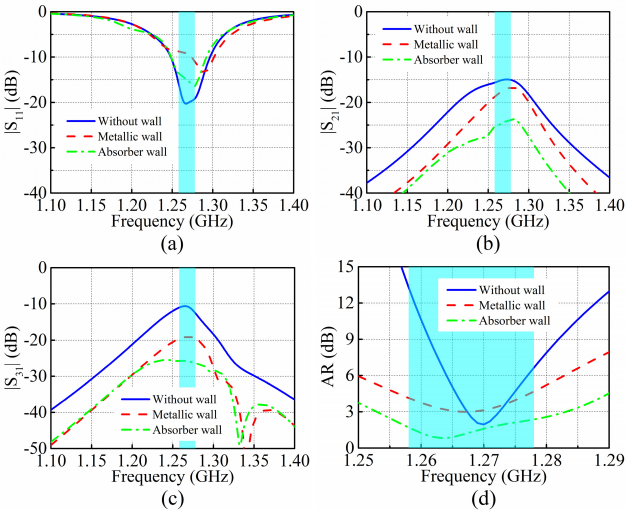

FIGURE 9. Simulated performance of the antenna array with different walls. (a) $|S_{11}|$. (b) $|S_{21}|$. (c) $|S_{31}|$. (d) Boresight AR of the Ant1.

the $|S_{21}|$ is about −17 dB and $|S_{31}|$ is no more than −19 dB. Last but not least, with the inclusion of the double-layer metamaterial absorber wall, both the $|S_{21}|$ and $|S_{31}|$ remain less than −25 dB within the BDS B3 band. As a result of the absorption feature of the metamaterial absorber, the inter-element isolation can be boosted by 10 dB and 15 dB, respectively, for the orthogonal-directed and parallel-directed antenna element pairs at the center frequency of 1268 MHz. In addition, an isolation enhancement of 7 dB is obtained for both orthogonal-directed and parallel-directed antenna element pairs with the employment of the double-layer metamaterial absorber wall as compared to the metallic wall. Most importantly, the boresight AR of the antenna element stays less than 3 dB across the target band in the presence of the metamaterial absorber wall. Consequently, the double-layer metamaterial absorber is demonstrated to be an effective approach to improve the inter-element isolation within a CP antenna array.

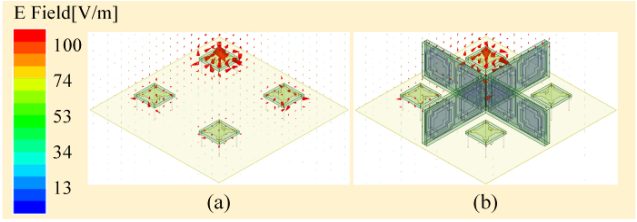

FIGURE 10. Simulated E-field distributions of the antenna array with and without the metamaterial absorber wall when the Ant1 is excited.

Fig. 10 illustrates the simulated *E*-field distributions at 1268 MHz for the antenna array in the absence and presence of the metamaterial absorber wall, when the Ant1 is excited. In contrast to that without any wall, the electromagnetic energy is mainly concentrated within the compartment where the Ant1 is located in the presence of the metamaterial absorber wall. The previous coupling electromagnetic energy are mostly absorbed by the metamaterial absorber wall. Thus, only minor electromagnetic energy are coupled to other

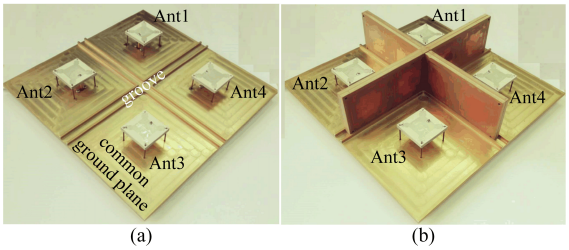

FIGURE 11. Prototype of the four-element CP antenna array. (a) Without any wall. (b) With the double-layer metamaterial absorber wall.

antenna elements. This can explain the effectiveness of the double-layer metamaterial absorber wall on suppressing the mutual coupling of the CP antenna array. Besides, more simulations demonstrate that the proposed isolation technique is also applicable to other different CP array configurations.

IV. EXPERIMENTAL RESULTS AND DISCUSSION

The antenna array has been fabricated and assembled as shown in Fig. 11. Copper pins are employed as the shorting pins. Sixteen holes with a radius of 0.5 mm and four holes with a radius of 0.75 mm are drilled in the common ground plane to settle the copper pins and probes, respectively. Four pieces of single-layer metamaterial absorber boards, including 1 × 4 cells, are sequentially soldered together to construct the double-layer metamaterial absorber wall. A notch with a width of 7.5 mm and a length of 22.5 mm is introduced on each metamaterial absorber board, allowing the two double-layer metamaterial absorber walls symmetrically crossed. The common ground plane of the whole antenna array is machined from a brass block and with a thickness of 3.0 mm. Moreover, two crossed shallow grooves of 3.0 mm high are also machined onto the common ground plane to fasten the metamaterial absorber wall. Also, the ground planes of the metamaterial absorber boards are soldered together as well as to the common ground plane during the assembly process. The antenna array prototype owns an overall volume of 190 mm × 190 mm ×48 mm, i.e. an electrical size $0.81\lambda_0 \times 0.81\lambda_0 \times 0.19\lambda_0$ at 1268 MHz. All the antenna elements are fed underneath the common ground plane using SMA connectors whose inner probes are soldered to the patch radiators.

Fig. 12(a) shows the simulated and measured $|S_{11}|$ of the prototype antenna array when the other ports are terminated with 50 Ω loads. The measured results well agree with the simulated ones, exhibiting that a 10 dB impedance bandwidth from 1240 MHz to 1288 MHz is obtained. Thanks to the rotational symmetry of the antenna array, the measured S_{22}, S_{33}, and S_{44} are similar to the measured S_{11}, which are not shown for brevity. The simulated and measured $|S_{21}|$ and $|S_{31}|$ are plotted in Figs. 12(b) and 12(c), respectively. Across the BDS B3 band, both $|S_{21}|$ and $|S_{31}|$ are kept below −22 dB. Compared with that without any wall, the $|S_{21}|$ and $|S_{31}|$ are reduced by about 8 dB and 11 dB, respectively. Therefore, the proposed double-layer metamaterial absorber wall can simultaneously mitigate the mutual coupling of the parallel-directed and orthogonal-directed antenna

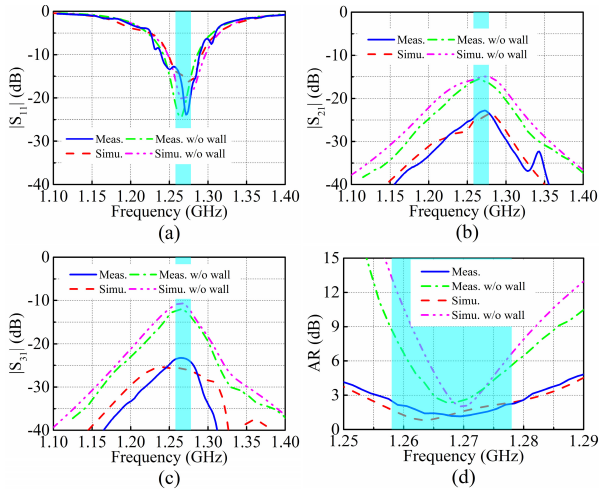

FIGURE 12. Simulated and measured S-parameters and boresight AR of the antenna array with and without the metamaterial absorber wall. (a) $|S_{11}|$. (b) $|S_{21}|$. (c) $|S_{31}|$. (d) Boresight AR of the Ant1.

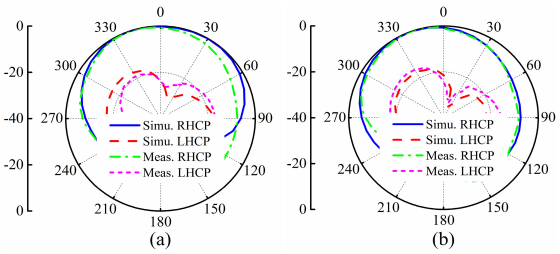

FIGURE 13. Simulated and measured radiation patterns of the Ant1 at 1268 MHz. (a) *x-z* plane. (b) *y-z* plane.

element pairs. Fig. 12(c) presents the simulated and measured boresight AR of the Ant1. It can be easily found that the prototype antenna achieves a 3 dB CP bandwidth from 1255 MHz to 1281 MHz. Discrepancies between the simulation and measurement results are mainly due to the fabrication tolerances and assembly imperfections.

The simulated and measured radiation patterns of the Ant1, both in the *x*-*z* and *y*-*z* planes at 1268 MHz, are given in Fig. 13. We can see that the measured results have a reasonable consistency with the simulated ones. Because of the scattering effect of the finite ground plane and the potential reflection of the metamaterial absorber wall, the beams squint approximately 20° from the boresight direction. The squint beam, however, hardly affects the anti-jam performance of the GNSS adaptive antenna in terms of null accuracy and depth. The measured peak realized CP gain is 2.3 dBic, which is 1.2 dB lower than that without any wall.

V. CONCLUSION

An isolation-enhanced four-element CP antenna array applicable to BDS anti-jam arrays has been designed, fabricated, and demonstrated. Four single-feed miniaturized CP antenna elements are orthogonally positioned to realize the antenna array. The mutual coupling between the antenna elements has been significantly reduced with the use of the proposed double-layer metamaterial absorber wall. For the presented prototype antenna array fitting within an overall footprint size of $0.81\lambda0 \times 0.81\lambda0$, the measured results exhibit that the isolation of the parallel-directed and orthogonal-directed antenna element pairs have been improved by 11 dB and 8 dB, respectively. At the same time, the antenna array achieves good CP property. The miniaturized antenna element and mutual coupling suppression technique also enable the implementation of more compact GNSS arrays.

REFERENCES

[1] E. D. Kaplan and C. J. Hegarty, *Understanding GPS: Principles and Applications*. Norwood, MA, USA: Artech House, 2006, pp. 243–299.
[2] R. L. Fante and J. J. Vaccaro, "Wideband cancellation of interference in a GPS receive array," *IEEE Trans. Aerosp. Electron. Syst.*, vol. 36, no. 2, pp. 549–564, Apr. 2000.
[3] J. R. Lambert, C. A. Balanis, and D. DeCarlo, "Spherical cap adaptive antennas for GPS," *IEEE Trans. Antennas Propag.*, vol. 57, no. 2, pp. 406–413, Feb. 2009.
[4] E. M. Friel and K. M. Pasala, "Effects of mutual coupling on the performance of STAP antenna arrays," *IEEE Trans. Aerosp. Electron. Syst.*, vol. 36, no. 2, pp. 518–527, Apr. 2000.
[5] H. T. Hui, "Reducing the mutual coupling effect in adaptive nulling using a re-defined mutual impedance," *IEEE Microw. Wireless Compon. Lett.*, vol. 12, no. 5, pp. 178–180, May 2002.
[6] S. Farsi, H. Aliakbarian, D. Schreurs, B. Nauwelaers, and G. A. E. Van denbosch, "Mutual coupling reduction between planar antennas by using a simple microstrip U-section," *IEEE Antennas Wireless Propag. Lett.*, vol. 11, pp. 1501–1503, 2012.
[7] H. L. Peng, R. Tao, W. Y. Yin, and J. F. Mao, "A novel compact dual-band antenna array with high isolations realized using the neutralization technique," *IEEE Trans. Antennas Propag.*, vol. 61, no. 4, pp. 1956–1962, Apr. 2013.
[8] S. C. Chen, Y. S. Wang, and S. J. Chung, "A decoupling technique for increasing the port isolation between two strongly coupled antennas," *IEEE Trans. Antennas Propag.*, vol. 56, no. 12, pp. 3650–3658, Dec. 2008.
[9] L. Zhao, F. Liu, X. Shen, G. Jing, Y.-M. Cai, and Y. Li, "A high-pass antenna interference cancellation chip for mutual coupling reduction of antennas in contiguous frequency bands," *IEEE Access*, vol. 6, pp. 38097–38105, 2018.
[10] C.-Y. Chiu, C.-H. Cheng, R. D. Murch, and C. R. Rowell, "Reduction of mutual coupling between closely-packed antenna elements," *IEEE Trans. Antennas Propag.*, vol. 55, no. 6, pp. 1732–1738, Jun. 2007.
[11] C.-M. Luo, J.-S. Hong, and L.-L. Zhong, "Isolation enhancement of a very compact UWB-MIMO slot antenna with two defected ground structures," *IEEE Antennas Wireless Propag. Lett.*, vol. 14, pp. 1766–1769, 2015.
[12] G. Zhai, Z. N. Chen, and X. Qing, "Enhanced isolation of a closely spaced four-element MIMO antenna system using metamaterial mushroom," *IEEE Trans. Antennas Propag.*, vol. 63, no. 8, pp. 3362–3370, Aug. 2015.
[13] F. Yang and Y. Rahmat-Samii, "Microstrip antennas integrated with electromagnetic band-gap (EBG) structures: A low mutual coupling design for array applications," *IEEE Trans. Antennas Propag.*, vol. 51, no. 10, pp. 2936–2946, Oct. 2003.
[14] E. Rajo-Iglesias, O. Quevedo-Teruel, and L. Inclan-Sanchez, "Mutual coupling reduction in patch antenna arrays by using a planar EBG structure and a multilayer dielectric substrate," *IEEE Trans. Antennas Propag.*, vol. 56, no. 6, pp. 1648–1655, Jun. 2008.
[15] Q. Li, A. P. Feresidis, M. Mavridou, and P. S. Hall, "Miniaturized double-layer EBG structures for broadband mutual coupling reduction between UWB monopoles," *IEEE Trans. Antennas Propag.*, vol. 63, no. 3, pp. 1168–1171, Mar. 2015.
[16] K. Buell, H. Mosallaei, and K. Sarabandi, "Metamaterial insulator enabled superdirective array," *IEEE Trans. Antennas Propag.*, vol. 55, no. 4, pp. 1074–1085, Apr. 2007.
[17] Z. Qamar, U. Naeem, S. A. Khan, M. Chongcheawchamnan, and M. F. Shafique, "Mutual coupling reduction for high-performance densely packed patch antenna arrays on finite substrate," *IEEE Trans. Antennas Propag.*, vol. 64, no. 5, pp. 1653–1660, May 2016.
[18] Z. Liu *et al.*, "Enhancing isolation of antenna arrays by simultaneously blocking and guiding magnetic field lines using magnetic metamaterials," *Appl. Phys. Lett.*, vol. 109, no. 15, Sep. 2016, Art. no. 153505.

[19] F. Liu, J. Guo, L. Zhao, X. Shen, and Y. Yin, "A meta-surface decoupling method for two linear polarized antenna array in sub-6 GHz base station applications," *IEEE Access*, vol. 7, pp. 2759–2768, 2018.
[20] A. A. Gheethan, P. A. Herzig, and G. Mumcu, "Compact 2 ÃČ—2 coupled double loop GPS antenna array loaded with broadside coupled split ring resonators," *IEEE Trans. Antennas Propag.*, vol. 61, no. 6, pp. 3000–3008, Jun. 2013.
[21] J. X. Li, J. W. Shi, K. Feng, Z. C. Xiao, J. Chen, and A. X. Zhang, "Isolation enhanced circularly polarized patch antenna array using modified electric-field-coupled resonator," *Int. J. RF Microw. Comput.-Aided Eng.*, vol. 11, Dec. 2018, Art. no. e21560.
[22] Y. Zhou, C. C. Chen, and J. L. Volakis, "Single-fed circularly polarized antenna element with reduced coupling for GPS arrays," *IEEE Trans. Antennas Propag.*, vol. 56, no. 5, pp. 1469–1472, May 2008.
[23] M. Chen and C.-C. Chen, "A compact dual-band GPS antenna design," *IEEE Antennas Wireless Propag. Lett.*, vol. 12, pp. 245–248, 2013.
[24] N. Nasimuddin, Y. S. Anjani, and A. Alphones, "A wide-beam circularly polarized asymmetric-microstrip antenna," *IEEE Trans. Antennas Propag.*, vol. 63, no. 8, pp. 3764–3768, Aug. 2015.
[25] S. Gao, Q. Luo, and F. Zhu, *Circularly Polarized Antennas*. Hoboken, NJ, USA: Wiley, 2013.
[26] J. M. Kovitz and Y. Rahmat-Samii, "Using thick substrates and capacitive probe compensation to enhance the bandwidth of traditional CP patch antennas," *IEEE Trans. Antennas Propag.*, vol. 62, no. 10, pp. 4970–4979, Oct. 2014.

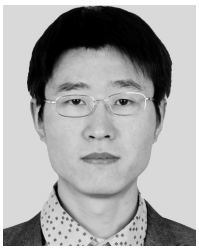

JUN ZHANG (S'12–M'13) received the B.S. degree in measurement and control technology and instrument from the Nanjing University of Science and Technology, Nanjing, China, in 2008, and the Ph.D. degree in instrument science and technology from Southeast University, Nanjing, in 2013. From 2013 to 2014, he was a Postdoctoral Research Fellow of the Postdoctoral Research Station of Control Science and Engineering, School of Automation, Southeast University, where he is currently an Associate Researcher with the Robotic Sensor and Control Laboratory, School of Instrument Science and Engineering. From 2014 to 2016, he was a Postdoctoral Research Fellow of the Robotics Institute, Carnegie Mellon University. His current research interests include bio-inspired robotics, rehabilitation robotics, mechatronics, multi-robot-based microsystem assembly, and wireless sensor networks.

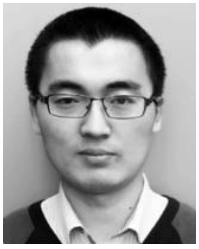

JIANXING LI (S'15–M'18) received the B.S., M.S., and Ph.D. degrees in electromagnetic field and microwave technology from Xi'an Jiaotong University, Xi'an, China, in 2008, 2011, and 2016, respectively, where he is currently a Lecturer with the School of Electronic and Information Engineering.

From 2014 to 2016, he was a Visiting Researcher with the Department of Electrical and Computer Engineering, Duke University, Durham, NC, USA, under the financial support from the China Scholarship Council. His current research interests include antennas, microwave and mmWave circuits, and metamaterials. He serves as a Reviewer for several international journals including the IEEE Access, *IET Electronics Letters*, the *International Journal of RF and Microwave Computer-Aided Engineering*, and the *International Journal of Electronics and Communications*.

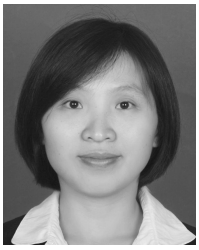

JUAN CHEN (M'18) received the Ph.D. degree in electromagnetic field and microwave technology from Xi'an Jiaotong University, Xi'an, China, in 2008, where she is currently a Professor with the Shenzhen Research School and the School of Electronic and Information Engineering.

From 2016 to 2017, she was a Visiting Researcher with the Department of Electrical and Computer Engineering, Duke University, Durham, NC, USA, under the financial support from the China Scholarship Council. Her current research interests include numerical electromagnetic methods, advanced antenna designs, and graphene theory and applications.